SCIENCE CHINA
Technological Sciences

August 2013 Vol.56 No.8: 2070–2080
doi: 10.1007/s11431-013-5274-6

An experimental investigation on the mechanism of fluid flow through single rough fracture of rock

JU Yang[1, 2*], ZHANG QinGang[3], YANG YongMing[3], XIE HePing[4], GAO Feng[2] & WANG HuiJie[3]

[1] *State Key Laboratory of Coal Resources and Safe Mining, China University of Mining and Technology, Beijing 100083, China;*
[2] *State Key Laboratory for Geomechanics and Deep Underground Engineering, China University of Mining and Technology, Xuzhou 221008, China;*
[3] *School of Mechanics and Civil Engineering, China University of Mining and Technology, Beijing 100083, China;*
[4] *Key Laboratory for Energy Engineering Safety and Disaster Mechanics of the Education Ministry, Sichuan University, Chengdu 610065, China*

Received January 31, 2013; accepted May 6, 2013; published online June 27, 2013

The structure of fractures in nature rock appears irregular and induces complicated seepage flow behavior. The mechanism and quantitative description of fluid flow through rock fractures is a difficult subject that has been greatly concerned in the fields of geotechnical, mining, geological, and petroleum engineering. In order to probe the mechanism of fluid flow and the effects of rough structures, we conducted a few laboratory tests of fluid flow through single rough fractures, in which the Weierstrass-Mandelbrot fractal function and PMMA material were employed to produce the fracture models with various fractal roughnesses. A high-speed video camera was employed to record the fluid flow through the entire single rough fracture with a constant hydraulic pressure. The properties of fluid flow varying with the fracture roughness and the influences of the rough structure were analyzed. The components of flow resistance of a single rough fracture were discussed. A fractal model was proposed to relate the fluid resistance to the fracture roughness. A fractal equivalent permeability coefficient of a single rough fracture was formulated. This study aims to provide an experimental basis and reference for better understanding and quantitatively relating the fluid flow properties to the structures of rock fractures.

seepage flow, single fracture, rough morphology, fractal description, rock fractures

Citation: Ju Y, Zhang Q G, Yang Y M, et al. An experimental investigation on the mechanism of fluid flow through single rough fracture of rock. Sci China Tech Sci, 2013, 56: 2070–2080, doi: 10.1007/s11431-013-5274-6

1 Introduction

Natural rock masses comprise of intact rock blocks and numerous fractures/joints that separate blocks and provide reservoirs and migration paths for oil, gas and water resources. The movement of oil, gas and water resources causes extra seepage forces acting on rock blocks, changing the stress distribution of rock masses. Mining and drilling activities disequilibrate the initial stress balance of rock masses, resulting in the deformation and failure of intact rocks as well as rock fractures, which, consequently, influences the properties of fluid flow and flow distribution in rock masses. This coupled stress and fluid flow mechanism of fractured rock masses has raised great concerns in both theory and practice. Statistical data from China indicate that more than 90% of water burst disasters in coal mines were closely related to water seepage of rock masses [1–3], more than 80% of coal gas outburst accidents were attributed to the dramatic change of permeability and stress distribution

*Corresponding author (email: juy@cumtb.edu.cn)

of rock masses caused by coal seam excavation and roadway construction [4–6], nearly 35%–40% of dam disasters were caused by water seepage uplift effect of rock masses [7–9], and more than 90% of rock slope failure associated with groundwater flow [8, 9]. In addition, the subsidence of mining surface, earthquake triggered by water reservoir construction, geological sequestration of nuclear waste, and underground storage of CO_2 are also related to the subjects of rock fracture evolution and the coupled stress-fluid flow interaction. Thus, an accurate knowledge and description of the behavior of fluid flow and the interaction mechanism of stress and fluid flow are of great significance to solving these engineering problems.

Roughly, the permeability of real rock masses has two components: the permeability of intact blocks and the permeability of rock fractures (including single fracture and fracture network). An intact block features the lower permeability comparing with the macro rock fractures. As many engineering disasters are closely related to the behavior of fluid flow through macro fractures, much more attentions have been paid to the properties of fluid flow through a single fracture and fracture network as well. Lots of hydro-mechanical coupling models including theoretical and numerical models were proposed [10–46]. However, as research continues, scientists and engineers are increasingly aware of many fundamental problems that are far away from satisfactory solutions. For instance, rock fractures form a spatial network comprising numerous randomly distributed, crossed single fractures. The coupled stress and flow properties of rock masses highly depend on the behavior of fluid flow through a single fracture and the roadmap that fluid disperses over the entire fracture network. The spatial distribution and interconnectivity of fractures as well as the properties of fluid flow through a single fracture essentially determine the overall permeability and the flow distribution of rock masses. Hence, a satisfactory stress and fluid flow coupling model requires at least 1) adequate characterization of fluid flow through a single fracture, 2) an accurate knowledge of the optimal roadmap that fluid follows through the entire network, and 3) proper description of the influences of the ambient stresses on the evolution of fracture network. Unfortunately, even for the fluid flow in a single fracture, the problem has not been settled with a satisfactory solution due to the following circumstances.

First of all, real fractures present irregular morphology, of which the characteristics including aperture, roughness, contact, and connectivity significantly influence the properties of fluid flow. It is hard to quantitatively describe the governing mechanism and the influencing factors of fluid flow through fractures. Little work is available on accurately characterizing the mechanisms that govern the coupled stress and fluid flow behavior of rock masses, such as surface morphology, fracture contact, connectivity, the correlation between Darcy flow or non-Darcy flow and fractures, and the interaction between fracture and fluid. Mostly, people have to use those macroscopically measurable data to establish the empirical models to express the permeability of rock varying with stresses (or strains). It is very hard to use these models to show and evaluate the intrinsic micro mechanisms, triggering conditions, and evolution processes of the coupled stress and fluid flow failure [10–46].

Secondly, cubic law, developed on the smooth parallel-plate assumption of a single fracture, is widely applied to analysis of the seepage flow of rock fractures. Numerous models based on the cubic law were established to estimate the flow properties of fractured rocks under exerted stresses [12–16, 18–24, 30, 31, 34–46]. Unfortunately, a real rock fracture appears to be rough, irregular, which does not meet the assumption of being smooth as postulated in the parallel-plate model. If the exerted stress is low and the fracture aperture is big enough, the cubic law, to some extent, could represent the behavior of seepage flow through fracture. Once the exerted stress arises so that more areas of the fracture surface come into contact, the assumption does not apply. The seepage flow is dominated by the morphology and the connectivity of the passageway formed by the untouched fracture surface. The seepage flow occurs in a so-called dominant passageway. In order to adapt to such a circumstance, Tsang et al. [43, 45] proposed a channel model for fluid flow through a tight fracture subjected to high stresses. However, the profile of the contacted surface which stresses apply to appears to be so irregular that it becomes extremely difficult to accurately define the channel wall structure and the seepage flow both in mathematics and in physics. Application of the channel model is therefore restricted seriously [12]. Lacking knowledge and experimental proofs about the behavior of fluid flow in an irregular fracture plays a constraining role in developing an accurate model taking into account the effects of rough structures on the fluid flow of rock factures under stresses.

Thirdly, in addition to the fracture morphology, the state of stress greatly influences the seepage flow through a single rough fracture as well. To date, many investigations on the effects of normal stresses [12, 15, 23–25, 30, 31, 34, 39, 44] have been carried out, but few about the influences of shear stresses. No thorough study about the effects of fracture deformation caused by shear stresses on the seepage flow is available [47–50], let alone the seepage mechanism of fractures under triaxial stresses [36, 38].

Fourthly, some investigators adopted the morphological parameters such as surface roughness, fractal dimension, contact surface shape, and contact area to characterize the morphological effects of a fracture [51–62]. Owing to the differences in experimental techniques and numerical methods, the conclusions about the effects of fracture roughness are evidently diverse, even opposite, between various investigations. Further study and experiments are needed to clarify the claims of the effects of rough structure and its evolution of fractures on the seepage flow of rock

under applied stresses.

Therefore, in order to probe the relationships between rough structure and seepage mechanism, we performed a few tests of water flow through single fractures. A single rough fracture model was produced using the Weierstrass-Mandelbrot fractal function and transparent PMMA materials. The width of the fracture and the water head difference were set to be constant, which was designed to figure out the effect of roughness on the seepage behavior in a single fracture. A high-speed video camera was used to capture the water flow in the rough fracture driven by hydraulic pressures, based on which the properties of water flow varying with fracture roughness and the influences of rough structure were discussed. The components of flow resistance were analyzed and a fractal model relating the flow resistance and the fracture roughness was established. The fractal equivalent permeability coefficient of a single rough facture was derived. This study aimed to provide an experimental basis and reference for accurately understanding and describing the correlation between the mechanism of seepage flow and the rough structure of a rock fracture.

2 Tests of water flow

2.1 Fractal models of single rough fractures

Figure 1 illustrates a set of transparent rectangle plates made of PMMA materials, embracing single rough fractures with various fractal dimensions. The plate scales 200 mm long, 100 mm wide, and 20 mm think. The rough morphology of a fracture is characterized by the fractal dimension D. Different fractal dimensions were used to examine the influence of surface roughness on the mechanism of water flow in the fracture, i.e., D_0=1.0, D_1=1.10, D_2=1.20, D_3=1.30, D_4=1.40, and D_5=1.50, respectively, among which D_0=1.0 represents the case of a smooth, flat fracture. The bigger the fractal dimension, the higher the surface roughness of the fracture. The fracture of a constant aperture was etched out using a laser cutter controlled by computer moving along the trajectory of a fractal curve defined by the following *Weierstrass-Mandelbrot* fractal function [63–65]

$$W(t)=\sum_{n=-\infty}^{\infty}(1-e^{ib^n t})\mathrm{e}^{i\varphi_n}/b^{(2-D)n}, \tag{1}$$

where constant b is a real number greater than 1.0, reflecting the deviation degree that a curve deviates from a straight line, φ_n represents an arbitrary phase angle, and the fractal dimension $D\in(1,2)$. Taking the real part of $W(t)$ as the fractal governing function $C(t)$ yields

$$C(t)=ReW(t)=\sum_{n=-\infty}^{\infty}(1-\cos b^n t)/b^{(2-D)n}. \tag{2}$$

Function $C(t)$ refers to a continuous, non-differentiable function with the fractal dimension D complying with

$$D_{HB}-(B/b)\leqslant D\leqslant D_{HB}, \tag{3}$$

where B is a real number, and D_{HB} refers to the Hausdorff-

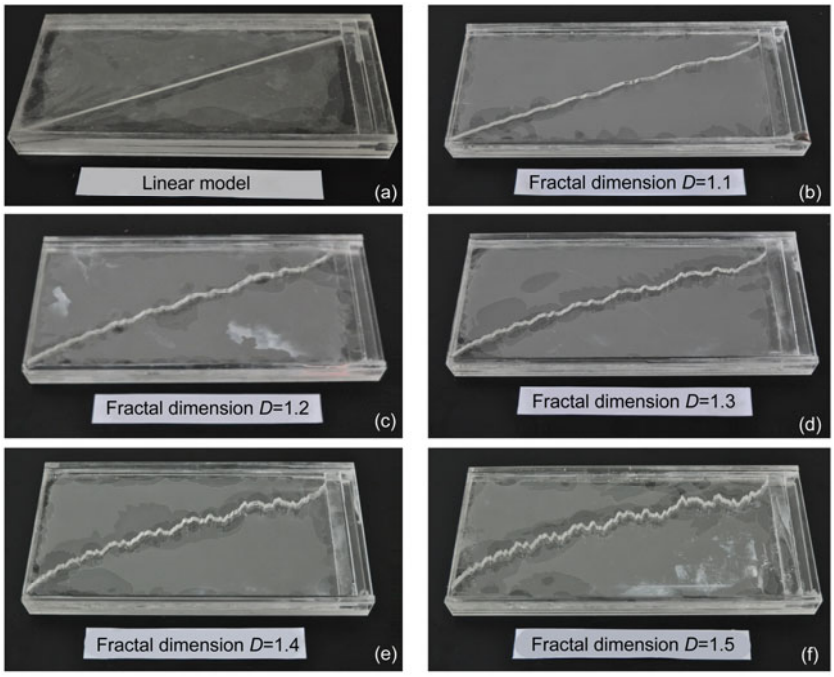

Figure 1 PMMA models of the rough single fractures with various fractal roughnesses. From (a)–(f), the fractal dimension D is equal to 1.0, 1.1, 1.2, 1.3, 1.4, and 1.5, respectively, where D=1.0 represents the smooth, flat fracture.

Besicovitch dimension.

MATLAB programming code was first used to generate the fractal curve $C_i(t)$ with a varying dimension. Then, the laser cutter etched out the fracture on the transparent PMMA plate along with the trajectory of curve C_i(t). The fractal indentation has a uniform depth of 5.0 mm and a width B of 2.0 mm, as shown in Figure 2. In order to stress the influences of roughness of fracture and to easily compare with the results of a straight, flat fracture straight, we set parameter b in the fractal function to be 1.4. Table 1 lists the total length of the fractal trajectory of a rough fracture determined using MATLAB tool based on eq. (2), and $L(D_i)$ refers to the total length of the fractal trajectory. Figure 2 depicts the local structure of the curve and the dimensions of the cross -section that water flows across. The total area of the cross-section meets A=10 (mm)^2.

2.2 Experimental procedure and measuring technique

Figure 3 pictures the assembled fracture model consisting of a horizontal plate and a vertical water tank, of which the dimensions of each part are indicated. The horizontal module embraces a rough fracture with a designated fractal dimension. All components of the model are made of transparent PMMA so that the water flow can be easily viewed and photographed. A sluice gate is located between the horizontal module and the vertical module. When testing, we first assembled the horizontal plate and the vertical water tank, and then sealed all joints with sealant to prevent water leak. The assembled model was placed on a horizontal flat desktop to ensure the water outlet and inlet of the fracture component to be on the same horizontal level. We poured

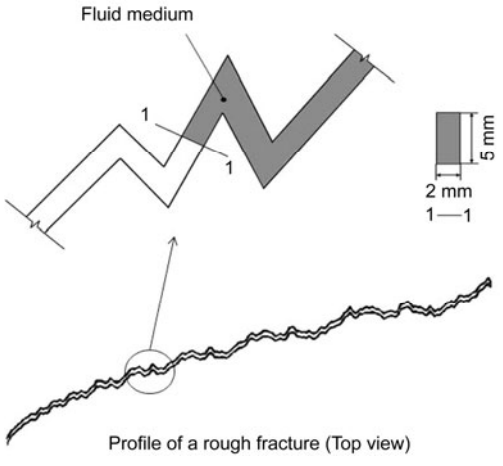

Figure 2 Diagram of the detailed structure of a fractal fracture and the dimensions of the cross-section that water flows through.

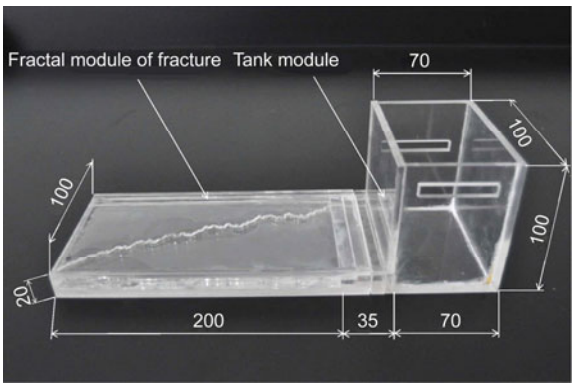

Figure 3 Panorama view of the integrated structure of seepage flow model and its components. The unit of size of each part refers to mm.

pure water into the water tank and added a few drops of red ink as a flow indicator. Lifting the sluice gate allows inked water to flow through the entire single fracture. The instantaneous flow process in the fracture was recorded and imaged using a high-speed digital video camera. For a single fracture with a specific fractal dimension, after being steady, a certain amount of water was measured using a measuring cup at the outlet of a fracture, and we recorded the number of seconds that the water took to run off the designated amount. The nominal flux rate and flow speed were derived according to the measurement. Repeating the procedure several times, we obtained the mean value of flux rates and flow speeds as the effective flux rate and the flow speed of water through the fracture with the specific fractal roughness. In order to keep the drop in water pressure head constant when flowing, we cut an additional outlet on the each sidewall of the water tank (see Figure 3) at 50 mm above the sluice gate, allowing extra water above that level to outflow from the tank as we watered uninterruptedly. This remains the drop in water pressure head ΔP to be as a constant of 490 Pa (considering the gravitational acceleration g= 9.8 m/s^2).

3 Experimental results and analysis

Figure 4 illustrates the water flow step-by-step in the rough fractures with various fractal dimensions recorded by a high-speed video camera with a speed of 500 frames per second. To investigate the influence of roughness, we arbitrarily selected several representative segments with an identical horizontal project length ΔL=10 mm. The interval distance between each segment was 30 mm, as shown in Figure 5. Using the number of video frames and the total length of path that water flowed, we worked out the average

Table 1 Total lengths of the profile trajectories of the fractal fractures with various fractal dimensions

Fractal dimension D_i	1.00	1.10	1.20	1.30	1.40	1.50
Total length $L(D_i)$ (mm)	217.70	225.50	237.30	264.40	321.30	400.40

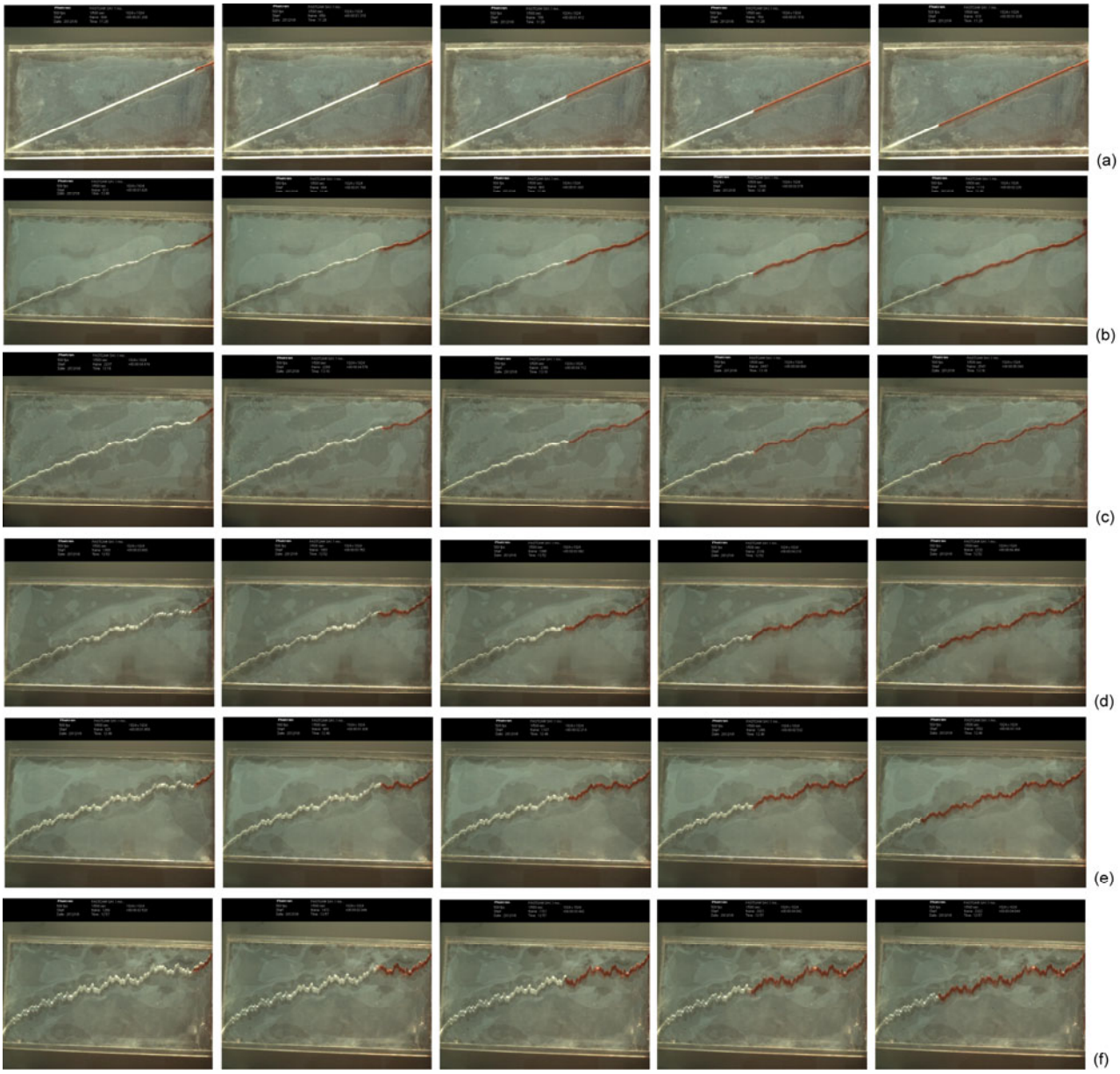

Figure 4 Instantaneous flows in the single fractures with different fractal roughnesses. From pictures (a) to (f), the fractal dimensions are equal to 1.0, 1.1, 1.2, 1.3, 1.4, and 1.5, respectively. D=1.0 stands for the smooth flat fracture. In each case with a distinct fractal dimension, from left to right, the horizontally projected length of the flow path is equal to 20, 50, 80, 110, and 140 mm, respectively.

speed of water flowing through the representative segment $\overline{v}_d$ and set it as the instantaneous speed of water flow at the end of the segment. Figure 6 shows the obtained average speeds $\overline{v}_d$ of water flow for different segments of the single fracture with various fractal dimensions. Figure 7 diagrams the mean speeds of water flow $\overline{V}_d$ through the entire fracture of various fractal dimensions.

The tests indicate that:

1) For a single fracture with a constant fractal dimension, although the rough structure of the selected segment appears different, the fluctuation of the average flow speed $\overline{v}_d$ seems to be negligible (see Figure 6). Moreover, the average flow speed in a smooth flat fracture whose fractal dimension D is equal to 1.0 will keep unchanged. This means that in terms of the single fracture of a constant fractal dimension the average speed $\overline{v}_d$ of water flow seems to be independent of its local structure.

2) Comparison between the rough fractures with various fractal dimensions implies that as the fractal dimension rises, i.e., the fracture roughness increases, the average speed of water flow $\overline{v}_d$ in any arbitrary segment will descend, and the mean speed of water flow $\overline{V}_d$ through the entire path of the fracture will linearly decrease as well (see Figures 6 and 7). Experimental data fitting indicates that the mean speed

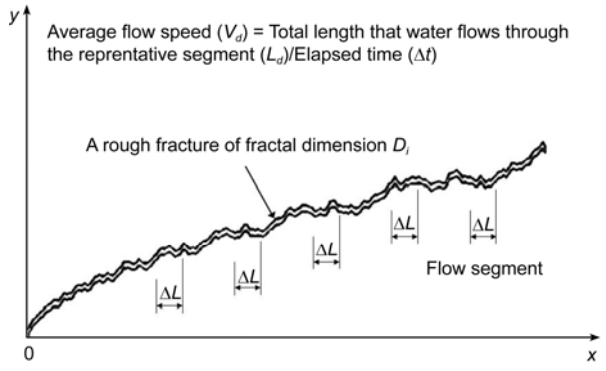

Figure 5 The average speed of water flow $\bar{v}_d$ through a representative segment. The horizontal project length of a segment ΔL equals 10 mm.

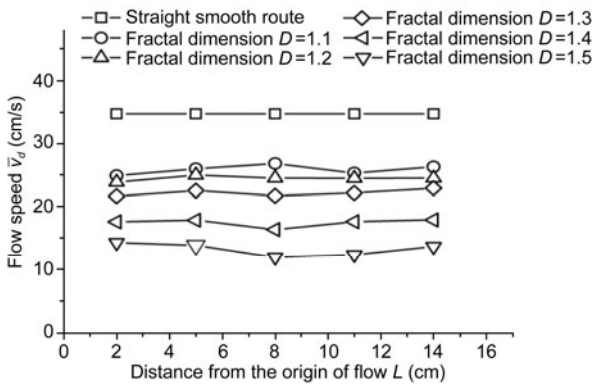

Figure 6 The average speeds of water flow $\bar{v}_d$ in the representative segments of single fractures with various fractal dimensions. The fractal dimensions of the rough fractures are 1.1, 1.2, 1.3, 1.4, and 1.5, respectively. D=1.0 refers to the fractal dimension of a smooth flat fracture.

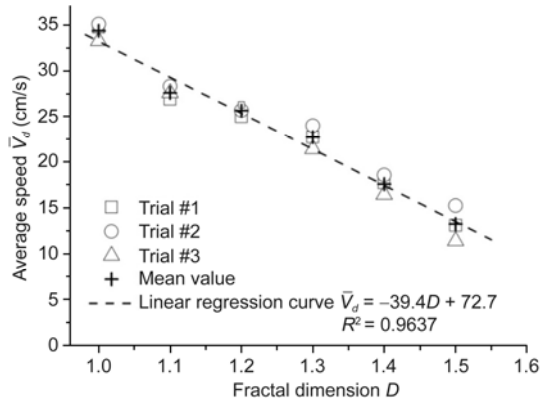

Figure 7 The mean speeds of water flow $\bar{V}_d$ through the entire single fracture with varying fractal dimensions.

of water flow $\bar{V}_d$ through the entire fracture linearly relates to its fractal dimension, which can be empirically formulated as

$$\bar{V}_d = 72.7 - 39.4D \ (\mathrm{cm/s}), \quad (1.0 \leqslant D \leqslant 1.8). \tag{4}$$

3) By the fluid mechanics theory [66, 67], the Reynolds number, *Re*, and the Euler number, *Eu*, of incompressible fluid may characterize the relationship between fluid viscous forces and inertial forces, and the relationship between fluid pressures and inertial forces, respectively. The Reynolds number *Re* and the Euler number *Eu* can be written, respectively as

$$Re = \frac{\rho v D}{\mu}, \tag{5}$$

$$Eu = \frac{\Delta p}{\rho v^2}, \tag{6}$$

where ρ, v, μ, Δp, and D refer to fluid mass density (g/m^3), fluid characteristic speed (m/s), fluid viscosity (N m^{-2} s^{-1}), head pressure difference between points of interest (Pa or N/m^2), and the characteristic length of flow path (m).

Taking the average speed of water flow in the representative segment of the single fracture as the characteristic speed, and defining the diagonal length of a cross-section as the characteristic length of flow path, we derived the Reynolds number R_e^d and the Euler number Eu^d of water flow through different rough fractures based on eqs. (5) and (6), respectively. Superscripts *d* in the Reynolds number and the Euler number represent the fractal dimension of a single rough fracture. Tables 2 and 3 list the obtained Reynolds number R_e^d and the Euler number Eu^d varying with the fractal dimension, respectively.

The calculation indicates that the Reynolds numbers R_e^d are less than 1800 for all rough fractures with various fractal dimensions. The greater the fractal dimension, i.e. the larger the roughness, of a single rough fracture, the smaller the Reynolds number. The Reynolds number linearly decreases with increasing the fractal dimension (see Figure 8). As the Reynolds number R_e^d of the flow is lower than the critical value 2000 [67, 68], the viscous force prevails, meaning that the flow in the rough fracture belongs to laminar flow. The more rough the path structure, the weaker the inertia effect, while the more prominent the laminar effect of flow. It is a reflection of the influence of rough structure of fracture on the flow mechanism. Moreover, the calculation of Euler numbers implies that the Euler number varies with the roughness of structure of flow path. The greater the fractal dimension, i.e. the bigger the roughness, the larger the Euler number. The Euler number increases nonlinearly with the increment of the fractal dimension of fracture. It indicates that the ratio between water pressure loss and dynamic pressure, i.e. the relative momentum loss rate or flow resistance rises as the fractal dimension increases, which reflects the influence of the rough structure of fracture on the resistance of the seepage flow.

Table 2 Reynolds number of water flow through varying rough fractures

Fractal dimension D_i	1.00	1.10	1.20	1.30	1.40	1.50
Reynolds number R_e^d	1455	1124	1045	950	742	549

Table 3 Euler number of water flow through varying rough fractures

Fractal dimension D_i	1.00	1.10	1.20	1.30	1.40	1.50
Euler number Eu^d	4.0	6.72	7.84	10.12	15.12	28.99

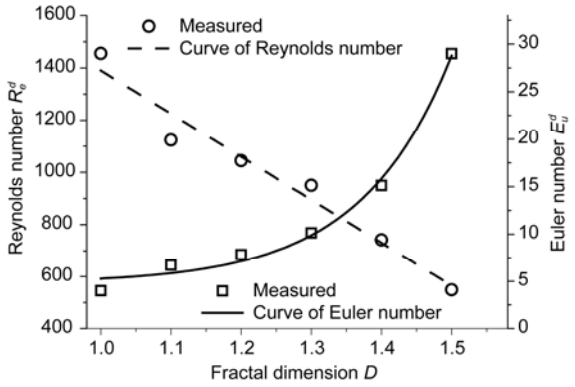

Figure 8 Reynolds number and Euler number varying with fractal dimension of rough fracture.

4 Flow resistance of rough fracture

In order to understand and describe the mechanism of how the rough structure affects the flow properties $\overline{V}_d$ or $\overline{v}_d$, we propose a fractal flow model to characterize the flow resistance varying with the roughness of single fracture.

According to the fluid mechanics theory [66–68], the flow resistance is proportional to the energy that flow dissipates, which means that the more the energy dissipated, the greater the resistance and the smaller the flow speed. Generally, flow resistance includes two parts, frictional resistance and local resistance. The frictional resistance results from the friction between the surface of structure and the fluid medium on a straight flow path, while the local resistance is attributed to the variation of flow direction at local places.

The frictional resistance, denoted by H_f, can be expressed in the *Fanning* equation [67, 68]:

$$H_f = \frac{\lambda L \rho v^2}{2d}, \tag{7}$$

where H_f represents the energy that fluid per unit volume consumes to overcome the fraction on a straight flow path. Parameter $\lambda = 64/R_e$ refers to the friction coefficient between fluid and path surface, L is the total length of the flow path, ρ is the fluid density, v means the mean flow speed, d stands for the equivalent characteristic length of the flow path, i.e. the equivalent diameter of the cross-section of the flow path when it is assumed to be circular. Table 5 lists the resulting frictional resistances of the flow through fractures with various roughnesses.

The local resistance as results of change of flow direction can be calculated by [66–68]:

$$H_l = \frac{\varepsilon \rho v^2}{2}, \tag{8}$$

where ε refers to the local resistance coefficient, satisfying

$$\varepsilon = \frac{\Delta p_c}{\Delta p} = 12\frac{\mu q l}{\Delta p \cdot B^3} = 12\frac{\theta \cdot R}{\Delta p \cdot R_e \cdot B}, \tag{9}$$

where θ stands for the bending angle of the local path where water flows around deflecting from the preceding straight path, R means the curvature radius of the centerline of the flow path, and B represents the fracture aperture, as shown in Figure 9.

The mechanisms of energy loss or local resistance as a result of the change of flow direction may be explained as follows. Consider that water flows through an arbitrary local place, denoted by $\boldsymbol{i}$, changing the flow direction from ① with instantaneous velocity $\boldsymbol{V}_i$ to ② with instantaneous velocity $\boldsymbol{V}_{i+1}$ (see Figure 9). The experimental results proved that the amplitude of instantaneous velocity remains unchanged, i.e., $|\boldsymbol{V}_i| = |\boldsymbol{V}_{i+k}| (k = 1, 2, \cdots)$. According to the momentum theorem, the difference vector of velocity $\Delta \boldsymbol{V}_i$ resulting from the change of flow direction can be expressed as

$$\Delta \boldsymbol{V}_i = \boldsymbol{V}_{i+1} - \boldsymbol{V}_i, \quad |\boldsymbol{V}_{i+1}| = |\boldsymbol{V}_i|,$$

$$|\Delta \boldsymbol{V}_i| = \sqrt{|\boldsymbol{V}_{i+1}|^2 + |\boldsymbol{V}_i|^2 - 2|\boldsymbol{V}_{i+1}| \cdot |\boldsymbol{V}_i| \cos\theta_i} = 2|\boldsymbol{V}_i| \sin(\theta_i/2). \tag{10}$$

From the above equations, one can easily find out that it is the difference vector of velocity that causes the energy dissipation and flow resistance. Table 4 lists the mean values of deflecting angles of local places in the five representative segments, θ_i, that we acquired using the self-developed computer program. The results imply that

Table 4 Average values of bending angles θ_i(°) of fractures with various fractal dimensions

Fractal dimension D_i	Segmt #1	Segmt # 2	Segmt # 3	Segmt # 4	Segmt # 5	Average
D=1.1	29	31	26	23	22	26
D=1.2	50	52	30	33	44	41
D=1.3	80	87	50	65	63	70
D=1.4	116	117	75	85	90	97
D=1.5	148	150	130	155	160	149

Note. That the segments are sorted in the order by which the water flows through, as shown in Figures 5.

the mean bending angle of rough fracture rises with increasing the fractal dimension. Using eq. (10), one can conclude that the rougher the structure of the flow path, the bigger the bending angle, and consequently, the larger the difference vector of velocity of flow, and the more significant the drop of flow speed in the fracture. Substituting the curvature radius R_i and the local fracture aperture B_i into eqs. (8) and (9) and summing all the results of each segments, one can gain the values of local resistance of single fractures with various fractal dimensions, as listed in Table 5.

In order to clarify the effect of roughness of fracture on flow velocity and flow resistance, we plot the flow velocity $\bar{V}_d$ and flow resistance H varying with the fractal dimension D of fracture in Figure 9.

The analyses aforementioned indicate that water flow behaves as a laminar flow owing to the influence of rough structure of the fracture, in which the viscous effect plays a dominant role, while the inertia effect is negligible. The flow resistance H of a single rough fracture mainly includes local resistance H_l which is attributed to the bending effect of the flow path, and the frictional resistance H_f which seems to be trivial. The flow resistance H rises proportionally as the fracture roughness increases (see Figure 10), showing a linear relationship between the flow resistance H and the fractal dimension D of the single rough structure

$$H = 38.4(D-1)+2.1 \quad (1.0 \leqslant D \leqslant 1.8),\ R^2 = 0.9350. \quad (11)$$

5 Fractal equivalent permeability coefficient of rough fracture

Taking account of the measured average flow flux Q per unit time and laminar flow effects, we define a fractal

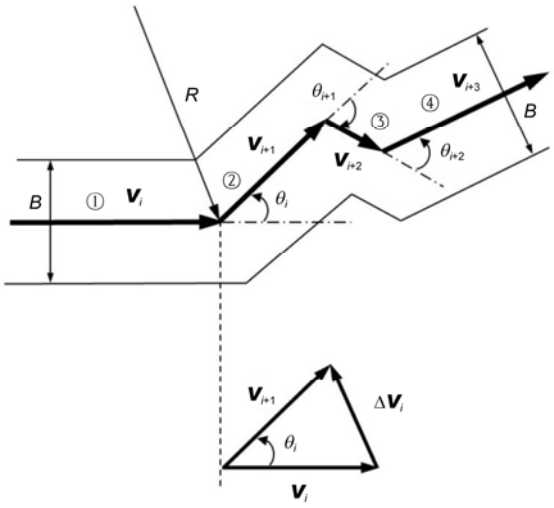

Figure 9 Illustration of the mechanism causing velocity difference and local resistance due to local bend of flow path.

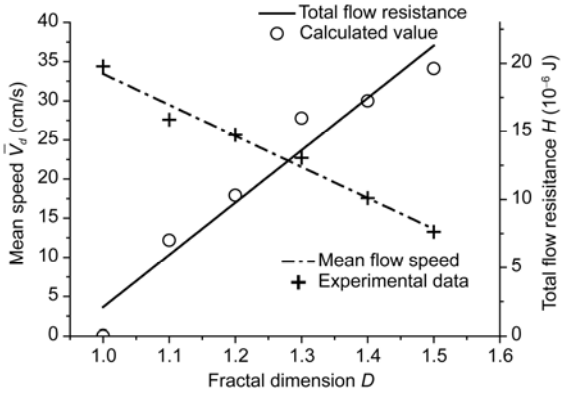

Figure 10 Variation of the mean flow speed $\bar{V}_d$ and the total resistance H of fracture varying with fractal dimension.

Table 5 Results of frictional resistance, local resistance, and total resistance of fractures with various fractal dimensions

Fractal dimension D_i	Local resistance H_l (10^{-6} J)	Frictional resistance H_f (10^{-9} J)	Total resistance H (10^{-6} J)
D=1.00 (smooth fracture)	0.00	0.012	0.012
D=1.10	7.01	0.017	7.027
D=1.20	10.30	0.020	10.320
D=1.30	15.97	0.027	15.997
D=1.40	17.25	0.051	17.301
D=1.50	19.62	0.097	19.717

Table 6 Fractal equivalent permeability coefficient K_{equ}^{d} of the single rough fracture

Fractal dimension D	1.0	1.1	1.2	1.3	1.4	1.5
Fractal equivalent permeability coefficient K_{equ}^{d} (mD)	260.92	146.32	90.79	58.97	40.02	25.53

equivalent permeability coefficient of a single rough fracture as follows to quantify the influence of a rough structure on water flow through the single fracture

$$K_{equ}^{d}=\frac{\mu\cdot Q\cdot L^{d}}{\Delta P\cdot A}, \tag{12}$$

where K_{equ}^{d} represents the fractal equivalent permeability coefficient considering the fractal effects of rough structures. Q means the average flow flux per unit time. L^{d} refers to the total length of the rough fracture taking its fractal feature into account, which turns to be the nominal linear length when the fracture features a smooth structure. A is the cross-sectional area of the path through which the fluid flows. ΔP is the pressure difference between the outlet and inlet of path. Table 6 lists the resulting fractal equivalent permeability coefficients of the rough fractures with various fractal dimensions using the experimental data. Figure 11 plots the fractal equivalent permeability coefficient varying with the fractal dimension.

From the measurement and Figure 11, one can easily formulate the following nonlinear relationship between the fractal equivalent permeability coefficient K_{equ}^{d} of a single fracture and the fractal dimension D of its rough structure

$$K_{equ}^{d}=\mathrm{e}^{11.5-6D}+16.7\ \ (\mathrm{mD}),\quad (1.0\leqslant D\leqslant 1.8). \tag{13}$$

6 Conclusions

In summary, we can get the following conclusions.

1) For a single fracture with a constant fractal dimension, although the rough structure of the selected path segment is different, the average flow speed $\overline{v}_{d}$ does not change much, implying that the average flow speed $\overline{v}_{d}$ is independent of its local structural morphology. As the fractal dimension of the rough structure rises, i.e., the roughness increases, the average flow speed $\overline{v}_{d}$ of a local path decreases. Meanwhile, the average flow speed $\overline{V}_{d}$ through the entire path of the fracture linearly decreases as the fractal dimension increases.

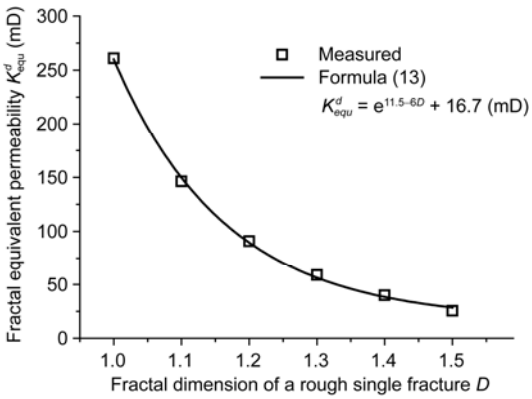

Figure 11 The fractal equivalent permeability coefficient of fractures varying with the fractal dimension of rough structure.

2) The Reynolds number of water flow linearly decreases with the increment of the fractal dimension of the fracture structure. The measured Reynolds number is smaller than the critical value, meaning that the water flow in the rough fracture belongs to a laminar flow, the viscous effect prevails. The rougher the structure of the fracture, the weaker the inertia effect, and the more significant the laminar effect of the flow. This is a reflection of the influence of roughness of fracture structure on the mechanism of fluid flow.

3) The Euler number of water flow varies with the roughness of structure of the flow path. The Euler number ascends nonlinearly with the increment of the fractal dimension of the fracture structure. The greater the fractal dimension, the more the energy loss and the larger the flow resistance. This phenomenon reflects the influence of rough structure of fracture on the resistance of flow through a single rough fracture.

4) The resistance of water flow through a single rough fracture is mainly attributed to the local resistance resulting from the local bending effect of the flow path. The frictional resistance seems to be negligible. The flow resistance proportionally rises as the fracture roughness increases. A fractal model is proposed to linearly relate the flow resistance to the fractal dimension D of the single rough structure.

5) A fractal equivalent permeability coefficient K_{equ}^{d} is defined to quantify the influence of a rough structure on water flow through the single rough fracture. An empirical model relating the fractal equivalent permeability coefficient to the fractal dimension of the rough structure is formulated. It is shown that the permeability of the single rough fracture exponentially rises with the fracture roughness increasing.

It is noteworthy that this study focuses on the influences of structural roughness of single fractures on the mechanisms of fluid flow. Further study is necessary to verify whether the findings that we concluded are appropriate for evaluating the behavior of seepage flow of viscous fluid or the behavior subject to applied stresses.

This work was supported by the National Science Funds for Distinguished Young Scholar of China (Grant No. 51125017), the National Basic Research Program of China (Grant Nos. 2010CB226804, 2011CB201201), the National Natural Science Foundation of China (Grant No. 50974125), the International Cooperation Project of Ministry of Science & Technology of China (Grant No. 2012DFA60760-2), and NSFC International Cooperation and Exchange Program (Grant No. 51120145001).

1 Zhang L H, Zhang Y C. The characteristic and general condition of coal mine water-bursting calamity in China (in Chinese). China Min Mag, 2008, 17: 44–46
2 Yu J C, Liu Z X, Liu S C, et al. Theoretical analysis of mine transient electromagnetic method and its application in detecting water burst structures in deep coal stope (in Chinese). J China Coal Society, 2007, 32: 818–821
3 Hu W Y. Mine Water Control Theory and Method (in Chinese). Beijing: Coal Industry Press, 2005
4 Zhou X Q, Chen G X. The probability analysis of occurrence causes of extraordinarily serious gas explosion accidences and its revelation (in Chinese). J China Coal Society, 2008, 33: 42–46
5 Zhou S N, Lin B Q. The Control Theory and the Gas Power Control Technology of Coal Mine Disaster Prevention (in Chinese). Beijing: Science Press, 2007
6 Fu J H, Cheng Y P. Situation of coal and gas outburst in China and control countermeasures (in Chinese). J Mining Safety Eng, 2007, 24: 253–259
7 He F, Wang L G, Wang Z W, et al. Experimental study on creep-seepage coupling law of coal (rock) (in Chinese). J China Coal Society, 2011, 36: 930–933
8 Wang H J. Study on Seepage Flow and control of deep and thick overburden of sluice foundation in the JinPin II hydropower station (in Chinese). Disssertation of Masteral Degree. Chengdu: Chengdu University, 2005
9 Wu Y Q, Zhang Z Y. An Introduction of Rock Mass Hydraulics (in Chinese). Chengdu: The University of Southwest Jiao Tong Press, 1995
10 Liu Q S, Wu Y X, Liu B. Discrete element analysis of effect of stress on equivalent permeability of fractured rock mass (in Chinese). Chin J Rock Mech Eng, 2011, 30: 176–183
11 Su B Y, Zhang W J, Sheng J C, et al. Study of permeability in single fracture under effects of coupled fluid flow and chemical dissolution (in Chinese). Rock Soil Mech, 2010, 31: 3361–3366
12 Xiong X B, Zhang C H, Wang E Z. A review of steady state seepage in a single fracture of rock (in Chinese). Chin J Rock Mech Eng, 2009, 28: 1839–1847
13 Zhang H C. Seepage-stress coupled model of heterogeneous and random fractured rock mass (in Chinese). J China Coal Society, 2009, 34: 1460–1464
14 Baghbanan A, Jing L R. Stress effects on permeability in a fractured rock mass with correlated fracture length and aperture. Int J Rock Mech Min Sci, 2008, 45: 1320–1334
15 Zhu Y H, Liu X R, Liang N H, et al. Current research and prospects in modeling seepage field in fractured rock mass (in Chinese). J Engng Geol, 2008, 16: 178–183
16 Li B, Jiang Y J, Koyama T, et al. Experimental study of the hydro-mechanical behavior of rock joints using a parallel-plate model containing contact areas and artificial fractures. Int J Rock Mech Min Sci, 2008, 45: 362–375
17 Jiang Y J, Li B, Wang G, et al. New advances in experimental study on seepage characteristics of rock fractures (in Chinese). Chin J Rock Mech Eng, 2008, 27: 2377–2386
18 Liu Z Q, Zhang Z Q. A review on the state of art of the saturated seepage-stress coupling models in rock mass (in Chinese). Adv Mech, 2008, 28: 585–600
19 Baghbanan A, Jing L R. Hydraulic properties of fractured rock masses with correlated fracture length and aperture. Int J Rock Mech Min Sci, 2007, 44: 704–719
20 Liu J S, Sheng J C, Polak A, et al. A fully-coupled hydrological-mechanical-chemical model for fracture sealing and preferential opening. Int J Rock Mech Min Sci, 2006, 43: 23–36
21 Zhang W J, Zhou C B, Li J P, et al. Research progress of experimental study on seepage characteristic of fractured rock masses (in Chinese). Rock Soil Mech, 2005, 26: 1517–1524
22 Hudson J A, Stephansson O, Andersson J. Guidance on numerical modeling of thermo-hydro- mechanical coupled processes for performance assessment of radioactive waste repositories. Int J Rock Mech Min Sci, 2005, 42: 850–870
23 Yang T H, Tang C A, Xu T, et al. The Seepage Properties of the Theory and the Application of The Model of Rock Failure Process (in Chinese). Beijing: Science Press, 2004
24 Mink B, Rutqvist J, Tsang C F, et al. Stress-dependent permeability of fractured rock masses: A numerical study. Int J Rock Mech Min Sci, 2004, 41: 1191–1210
25 Yasuhara H, Elsworth D, Polak A. The evolution of permeability in a natural fracture: The significant role of pressure solution. J Geophys Res, 2004, 109: 1029–1029
26 Miu X X, Liu W Q, Chen Z Q. Seepage Theory of Mining Rock (in Chinese). Beijing: Science Press, 2004
27 Zhang G X, Wu X X. Influence of seepage on the stability of rock slope—coupling of seepage and deformation by DDA method (in Chinese). Chin J Rock Mech Eng, 2003, 22: 1269–1275
28 Rutqvist J, Stephansson O. The role of hydromechanical coupling in fractured rock engineering (in Chinese). Hydrogeol J, 2003, 11: 7–40
29 Liang W G, Zhao Y S, Li Z P. The coupled mathematical model and numerical simulation of hydraulic fracturing and dissolving in rock salt (in Chinese). Chinese J Geotech Eng, 2003, 25: 427–430
30 Wang Y. Coupling characteristic of stress and fluid flow within a single fracture (in Chinese). Chin J Rock Mech Eng, 2002, 21: 83–87
31 Liu C H, Chen C X. Testing study on seepage characteristic of a single rock fracture under two-dimensional stresses (in Chinese). Chin J Rock Mech Eng, 2002, 21: 1194–1198
32 Yang T H. Coupling analysis of seepage and stresses in rock failure process (in Chinese). Chinese J Geotech Eng, 2001, 23: 49–53
33 Zheng S H, Zhu W S. Theoretical analysis on a coupled seepage damage model of fractured rock mass (in Chinese). Chin J Rock Mech Eng, 2001, 20: 156–159
34 Wang Y, Xu Z Y, Su B Y. Complete coupled analysis of fluid flow and elastoplastic stress in complicated fractured rock masses (in Chinese). Chinese J Geotech Eng, 2000, 19: 177–181
35 Xiao Y X, Lee C F, Lee S J. Assessment of an equivalent porous medium for coupled stress and fluid flow in fractured rock. Int J Rock Mech Min Sci, 1999, 36: 871–881
36 Zhao Y S, Yang D, Zheng S H, et al. Water seepage experiment of rock property of rock fracture under the three dimension stress (in Chinese). Sci China Ser E-Tech Sci, 1999, 29: 133–136
37 Zhu Z D. The unstable fractured rock mass seepage field and the damage field coupling analysis model (in Chinese). Hydrogeol Eng Geol, 1999, 26: 35–42
38 Zheng S H，Zhao Y S，Duan K L. An experimental study on the permeability law of natural fracture under 3d stresses (in Chinese). Chinese J Geotech Eng, 1999, 18: 133–136
39 Zhang Y Z, Zhang J C. Experimental study of the seepage flow-stress coupling in fractured rock masses (in Chinese). Rock Soil Mech, 1997, 18: 59–62
40 Zhou C B, Xiong W L. A generalized cubic law for percolation in rock joints (in Chinese). Rock Soil Mech, 1996, 17: 1–7
41 Nicholl M J, Glass R J, Wheatcraft S W. Gravity-driven infiltration instability in initially dry non-horizontal fractures. Water Resour Res, 1994, 30: 2533–2546

42 Hestir K, Long J C S. Analytical expressions for the permeability of random two-dimensional Poisson fracture networks based on regular lattice percolation and equivalent media theories. J Geophys Res, 1990, 95: 21565–21581

43 Tsang Y W, Tsang C F. Channel model of flow through fractured media. Water Resour Res, 1987, 23: 467 –479

44 Liu J S. The seepage formulas of single fracture by the normal stress (in Chinese). Hydrogeol Engng Geol, 1987, 14: 28–32

45 Tsang Y W, Witherspoon P A. The dependence of fracture mechanical and fluid flow properties on fracture roughness and sample size. J Geophys Res, 1983, 88: 2359–2366

46 Kranz R L, Frankel A D, Engelder T, et al. The permeability of whole and jointed Barre granite. Int J Rock Mech Min Sci Geomech Abs, 1979, 16: 225–234

47 Grasselli G, Egger P. Constitutive law for the shear strength of rock joints based on three-dimensional surface parameters. Int J Rock Mech Min Sci, 2003, 40: 25–40

48 Olsson R, Barton N. An improved model for hydromechanical coupling during shearing of rock joints. Int J Rock Mech Min Sci, 2001, 38: 317–329

49 Esaki T, Du S, Mitani Y, et al. Development of a shear-flow test apparatus and determination of coupled properties for a single rock joint. Int J Rock Mech Min Sci, 1999, 36: 641–650

50 Yeo I W, De Freitas M H, Zimmerman, et al. Effect of shear displacement on the aperture and permeability of a rock fracture. Int J Rock Mech Min Sci, 1998, 35: 1051–1070

51 He Y L, Tao Y J, Yang L Z. Experimental research on hydraulic behaviors in a single joint with various values of JRC (in Chinese). Chin J Rock Mech Eng, 2010, 29: 3236–3240

52 Jiang Y J，Li B, Tanabashi Y. Estimating the relation between surface roughness and mechanical properties of rock joints. Int J Rock Mech Min Sci, 2006, 43: 837–846

53 Jeong W, Song J. A numerical study on flow and transport in a rough fracture with self-affine fractal variable apertures. Energ Source, 2008, 30: 606–619

54 Glover P W J, Hayashi K. Modelling fluid flow in rough fractures: application to the Hachimantai geothermal HDR test site. Phys Chem Earth, 1997, 22: 5–11

55 Sahimi M. Flow phenomena in rocks: from continuum models to fractals, percolation, cellular automata, and simulated annealing. Rev Modern Phys, 1993, 65: 1393–1534

56 Thompson M E. Numerical simulation of solute transport in rough fractures. J Geophys Res, 1991, 96: 4157–4166

57 Brown S R. Transport of fluid and electric current through a single fracture. J Geophys Res, 1989, 94: 9429–9438

58 Pan P Z, Feng X T, Xu D P, Shen L F, Yang J B. Modelling fluid flow through a single fracture with different contacts using cellular automata. Comput Geotech, 2011, 38: 959–969

59 Nemoto K, Watanabe N, Hirano N, et al. Direct measurement of contact area and stress dependence of anisotropic flow through rock fracture with heterogeneous aperture distribution. Earth Planetary Sci Lett, 2009, 281: 81–87

60 Cai J L, Zhou Z F. Review of seepage research in rough fractures (in Chinese). Site Investigation Sci Tech, 2009: 18–23

61 Zimmerman R W, Chen D W, Cook N G W. The effect of contact area on the permeability of fractures. J Hydrology, 1992, 139: 79–96

62 Zhang Q. Effects of contact area on the permeability of planar fractures. J Hohai Univer, 1994, 22: 57–64

63 Mandelbrot B B. The Fractal Geometry of Nature. New York: W H Freeman, 1982

64 Feder J. Fractals. New York: Plenum Press, 1988

65 Xie H P. Fractals in Rock Mechanics. Rotterdam: A. A. Balkema, 1993

66 Liu H N. Fluid mechanics (2nd ed) (in Chinese). Beijing: China Architect Building Press. 2004

67 Roberson J A, Crowe C T. Engineering Fluid Mechanics (3rd ed). Boston: Houghton Mifflin, 1985

68 Finnemore E J, Franzini J B. Fluid Mechanics with Engineering Applications (10th ed). New York: McGraw-Hill Companies Inc, 2002